Non-equilibrium longitudinal and transverse optical phonons in terahertz quantum cascade lasers

Miriam S. Vitiello,[1,a)] Rita C. Iotti,[2] Fausto Rossi,[2] Lukas Mahler,[3] Alessandro Tredicucci,[3] Harvey E. Beere,[4] David A. Ritchie,[4] Qing Hu,[5] and Gaetano Scamarcio[1,b)]
[1]*CNR-Istituto di Fotonica e Nanotecnologie UOS Bari and Dipartimento Interateneo di Fisica "M. Merlin," Università degli Studi di Bari, Via Amendola 173, 70126 Bari, Italy*
[2]*Dipartimento di Scienza Applicata e Tecnologia, Politecnico di Torino, Corso Duca degli Abruzzi 24, 10129 Torino, Italy*
[3]*NEST, CNR-Istituto Nanoscienze and Scuola Normale Superiore, Piazza san Silvestro 12, 56127 Pisa, Italy*
[4]*Cavendish Laboratory, University of Cambridge, Madingley Road, Cambridge CB3 0HE, United Kingdom*
[5]*Department of Electrical Engineering and Computer Science and Research Laboratory of Electronics, Massachusetts Institute of Technology, Cambridge, Massachusetts 02139, USA*

(Received 29 December 2011; accepted 3 February 2012; published online 27 February 2012)

We report on the experimental observation of non-equilibrium longitudinal (LO) and interface transverse-like (IF-TO) optical phonons populations associated with electron transport in resonant-phonon THz quantum-cascade lasers. The measured LO-phonon occupation numbers are in excellent agreement with the result of Monte Carlo simulations at a phonon in-plane wave number $q = 4.2 \times 10^{+4}\,cm^{-1}$, and they remain about 40% larger than the IF-TO ones. © *2012 American Institute of Physics*. [doi:10.1063/1.3687913]

In semiconductor heterostructures and related devices, the energy relaxation of carriers is mostly controlled by the electron-phonon interaction.[1] If the excess energy supplied to the electronic ensemble is sufficiently high, the electron cooling processes may generate non-equilibrium optical-phonon populations which, in turn, may cause substantial changes in the carrier relaxation kinetics.

The latter effects are expected to be very pronounced in quantum cascade lasers (QCLs) in which the light-emission mechanism involving intersubband transitions between quantized conduction band energy states exploits the electron-phonon interaction to achieve population inversion.

In a terahertz QCL, the energy relaxation of carriers proceeds via a combination of intra- and inter-subband transitions, while the dominant non-radiative *e-e*-scattering modifies the electron distribution among the laser subbands. However, when energetically permitted, as in the case of resonant-phonon active region designs,[2] the electron-optical phonon interaction may have a major role as inter-subband relaxation mechanism and may lead to the creation of a non-equilibrium optical phonon population.[3] Considering the potential energy drop per stage necessary for band structure alignment and the energies of the relevant optical phonons, in a resonant-phonon THz QCL,[2] each electron generates at least one optical phonon per stage. Since resonant-phonon THz QCL structures employ more than one hundred periods, a large rate of optical phonon generation can be achieved. This means that the inclusion of the phonon ensemble in the band structure engineering is necessary to give a more realistic description and control not only on the electronic processes and lifetimes but also on the phonon processes as well. In addition, the large hot-optical phonon generation achievable in principle in THz QC structures could be exploited to use similar structures as sources of quasi-monochromatic optical phonon distributions. Such a device would have potential applications for the generation of high-frequency phonon beams used in phonon optics, phonon spectroscopy, and nanostructures imaging.[4]

In the present letter, we report on the experimental observation of non-equilibrium optical phonon populations generated by electron transport in THz QCLs emitting at 3.2 THz.[5]

The investigated devices are based on GaAs/$Al_{0.15}Ga_{0.85}As$ quantum cascade heterostructures employing a resonant phonon gain medium design.[5,6] The active region, grown by molecular beam epitaxy on an undoped GaAs substrate, includes $N = 200$ periods for a total thickness of $\sim 10.8\,\mu m$ and is embedded between two contact GaAs layers. Their thickness/doping values are $80\,nm/5 \times 10^{18}\,cm^{-3}$ and $700\,nm/3 \times 10^{18}\,cm^{-3}$. A schematic diagram of the active region design is sketched in Fig. 1. At variance from chirped superlattice and bound-to-continuum designs relying on intra-miniband scattering and transport for depopulation of the lower radiative state, the investigated design uses resonant tunneling and subpicosecond longitudinal-optical (LO)-phonon scattering assisted depopulation. Moreover, the photon energy is smaller than the longitudinal-optical phonon one ($E_{LO} = 36\,meV$ in GaAs), thus thermally activated LO-phonon scattering leads to a rapid decrease of the upper state lifetime at an increasing temperature, which reduces the laser gain.

The wafer (sample a) was processed in a double-metal waveguide using gold-gold wafer bonding followed by substrate removal and processed into 82-μm wide ridges by wet etching. Devices were metalized before wafer bonding with Ti/Au (5 nm/700 nm) and the ridges were contacted with Ti/Au (5 nm/200 nm). 5-μm wide, 10-μm long top apertures have then been defined by optical lithography on top of each metalized ridge, and the 80-nm heavily doped upper cladding layer was removed by wet etching using the top metal

[a)]Present address: CNR Dipartimento di Materiali e Dispositivi – Largo E. Fermi 6, 50125 Firenze and NEST, CNR-Istituto Nanoscienze and Scuola Normale Superiore, Piazza San Silvestro 12, 56126 Pisa, Italy. Electronic mail: miriam.vitiello@sns.it.
[b)]Electronic mail: scamarcio@fisica.uniba.it.

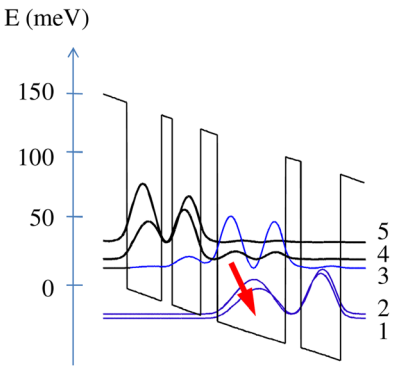

FIG. 1. (Color online) Conduction band schematic calculated using a self-consistent Schroedinger and Poisson solver. The four-well module is based on GaAs/$Al_{0.15}Ga_{0.85}As$ heterostructures. Beginning with the left injection barrier, the layer thicknesses in Å are 55/79/25/65/41/155/30/90. The 155 Å well is doped at $n = 1.9 \times 10^{16}\,cm^{-3}$, which yields a sheet density of $n = 3 \times 10^{10}\,cm^{-2}$ per module. The red arrow indicates the optical phonon assisted transition depleting the lower laser level.

contact as a mask. The latter procedure has the purpose of probing the population of phonon modes with different wavevector directions from both laser facet (in-plane k) and surface (k along the (001)-direction).

After processing, the samples were cleaved in 0.64-mm long cavities and indium soldered on copper mounts. In addition, non-lasing devices of comparable areas (sample b) and identical active region design were fabricated by optical lithography and wet etching in single plasmon-optical waveguides. The higher cavity losses of the single plasmon waveguides inhibit in this case the laser action.

The phonon population has been measured by a combination of microprobe band-to-band photoluminescence (PL) (Refs. 6–8) and micro-Raman spectroscopy.[3] PL and Raman spectra were recorded by focusing the 647-nm line of a Kr^+ laser, working in continuous mode, directly onto the QCL front facet, down to a spot of about 2-μm diameter by using an 80× long-working-distance plano-achromatic microscope objective lens. Raman experiments were performed in a backscattering configuration by probing the pumping laser on the laser facet and on a small aperture on the top surface in order to have access to both interface-transverse optical (IF-TO) or LO phonons, respectively. Indeed, wavevector conservation selection rules allow for interface phonon observation in backscattering from the sample edge. In contrast, LO phonons can only be observed in backscattering from the (001) surface.

The excitation wavelength has been chosen to avoid any resonant effect in the Raman spectra. At $\hbar\omega_L = 1.92\,eV$ only TO or transverse interface modes are not affected by electronic resonances, while to detect non-resonant LO phonons, a frequency $\hbar\omega_L = 2.60$ eV has been used. The absence of any resonant effect is confirmed by the measured value of the ratio between second order and first order intensities of the Raman spectrum (≈6%), being approximately equal to the expected thermal value.[3]

The devices were mounted into a helium-flow microcryostat and kept at a fixed heat sink temperature $T_H = 56\,K$ controlled with a calibrated Si-diode mounted close to the device. The sample position was varied using a two-dimensional translation stage with a 0.1-μm spatial resolution, along either the z or the x axis. The PL and Raman signals were dispersed using a 0.64-m monochromator and detected by a Si charge coupled device (CCD) cooled to 140 K. We used an interference notch filter to suppress the Rayleigh scattering and simultaneously record both Raman Stokes (S) and anti-Stokes (AS) spectra.

The measured Raman S/AS spectrum gives an estimate of the phonon population. In fact, the ratio ρ between the S/AS intensities for a given phonon mode is related with the phonon population via the relation,

$$N = \left[\rho \frac{\sigma_{AS}(\omega_L)}{\sigma_S(\omega_L)} \left(\frac{\omega_L + \omega_0}{\omega_L - \omega_0}\right)^4 - 1\right]^{-1}, \qquad (1)$$

where N is the phonon occupation number, ω_0 is the optical phonon frequency, $\sigma_s(\omega_L)$ and $\sigma_{As}(\omega_L)$ are the S and AS Raman cross sections at the laser frequency ω_L.[3] A ratio $\sigma_{AS}/\sigma_S = 1.04 \pm 0.015$ has been extracted from the measurement of the ratio of the AS/S intensities as a function of the heat sink temperature, by probing the device with zero current. The assessment of a non-equilibrium phonon population requires a comparison between the values of N extracted from Raman scattering with the thermal equilibrium values N_0. The latter information can be obtained using the microprobe PL technique exploited for the temperature mapping of THz QCLs.[9] The local lattice temperature of the device during operation was obtained from the shift of the PL spectrum recorded in the active region layers.[9] Starting from the effective lattice temperatures T_L, extracted from PL measurements, we then calculated the N_0 values from the expression: $N_0 = 1/(1 - e^{\frac{\hbar\omega}{k_B T_L}})$.

Figure 2 shows the dependence of the LO phonon population on the electrical power (P) dissipated in sample b. A considerable generation of hot LO phonons is evident from the comparison with the steady state population number.

In order to have a theoretical insight into the complex non-equilibrium dynamics of the interacting electron-phonon system within a semiclassical framework, one should consider Boltzmann equations involving the coupling of electrons and phonons. This task is, however, extremely demanding, since it would require the inclusion of both acoustic and optical modes, considering quantum size effects. To focus on the main physical aspects of the energy redistribution between

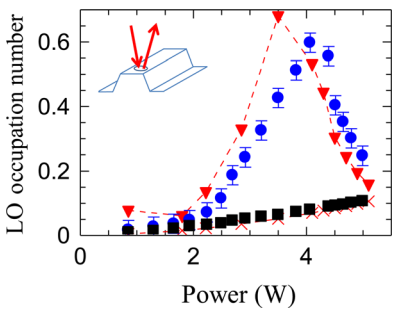

FIG. 2. (Color online) Experimental (●) and theoretical (▼) longitudinal optical phonon occupation numbers N in a mesa device (on sample b) as a function of the electrical power (P), displayed together with the measured (■) and calculated (×) equilibrium phonon population N_0. The dashed curve is a guide for the eye. The Kr^+ laser power density is $P_0 = 3 \times 10^4\,W \cdot cm^{-2}$, and the heat sink temperature is 56 K.

charge carriers and lattice degrees of freedom in resonant-phonon device designs, we have, therefore, considered the full electron subsystem, i.e., the complete set of active-region and injector subbands – interacting with out-of-equilibrium bulk (dispersionless) LO-phonon modes. The latter are assumed to decay anharmonically into thermalized acoustic modes (lattice thermal bath) by means of a phenomenological lifetime τ.[10] In particular, within the Fermi's golden rule approximation, the LO-phonon interaction translates into the following term in the electronic Boltzmann transport equation for the distribution function $f_{\nu\mathbf{k}}$ of the single-electron state in subband υ and with wave vector $\mathbf{k}$,

$$\left.\frac{d}{dt}f_{\nu\mathbf{k}}\right|_{e-LO} = \sum_{\mathbf{q}^{\pm}}\left(N_{\mathbf{q}}+\frac{1}{2}\pm\frac{1}{2}\right)\sum_{\nu'\mathbf{k}'}\left[(1-f_{\nu\mathbf{k}})P^{\mathbf{q}^{\pm}}_{\nu\mathbf{k},\nu'\mathbf{k}'}f_{\nu'\mathbf{k}'} - (1-f_{\nu'\mathbf{k}'})P^{\mathbf{q}^{\pm}}_{\nu'\mathbf{k}',\nu\mathbf{k}}f_{\nu\mathbf{k}}\right], \tag{2}$$

here, $N_{\mathbf{q}}$ is the phonon population of the LO-modes with wave vector $\mathbf{q}$, $P_{\upsilon\mathbf{k},\upsilon'\mathbf{k}'}{}^{\mathbf{q}^{\pm}} = (2\pi/\hbar)\,|g_{\upsilon\mathbf{k},\upsilon'\mathbf{k}'}{}^{\mathbf{q}^{\pm}}|^2\,\delta(\varepsilon_{\upsilon\mathbf{k}} - \varepsilon_{\upsilon'\mathbf{k}'} \pm \varepsilon_{\mathbf{q}})$, where $g_{\upsilon\mathbf{k},\upsilon'\mathbf{k}'}{}^{\mathbf{q}^{\pm}}$ is the Frölich carrier-phonon coupling coefficient, and the sign $\pm$ refers to emission (+) or absorption (−) processes. To properly model the carrier-phonon interacting systems, the Boltzmann transport equation for the electron subsystem, with the contribution in Eq. (1), goes together with the following phonon counterpart:

$$\frac{d}{dt}N_{\mathbf{q}} = \sum_{\pm}\pm\left(N_{\mathbf{q}}+\frac{1}{2}\pm\frac{1}{2}\right)\sum_{\nu\mathbf{k}\neq\nu'\mathbf{k}'}(1-f_{\nu\mathbf{k}})P^{\mathbf{q}^{\pm}}_{\nu\mathbf{k},\nu'\mathbf{k}'} - \frac{N_{\mathbf{q}}-N^{th}_{\mathbf{q}}}{\tau}, \tag{3}$$

where $N_{\mathbf{q}}$th is Bose-Einstein distribution at the lattice temperature T_L. The kinetic equations (2) and (3) are sampled by means of a Monte Carlo simulation scheme able to deal with a variable number of phonons on one side and a "charge conserving scheme" for the electrons on the other. The latter is obtained by imposing periodic boundary conditions. To properly account for relevant intra- as well as inter-subband scattering mechanisms, besides carrier-LO phonon scattering, we have also included carrier-carrier interaction in the electron dynamical equation. For the electron-electron interaction, here we employ the well-established time-dependent static-screening approach commonly used in Monte Carlo simulations of energy relaxation and transport phenomena in two-dimensional systems. Indeed, the impact of more refined screening models on the non-equilibrium many-body dynamics in these devices is still debated.[11] To limit the number of free-parameters, extrinsic, and strongly material/device dependent, scattering mechanisms, such as carrier-impurity and interface roughness,[11,12] have not been included in the present simulations. As far as the two phenomenological parameters of the model, τ and T_L, are concerned, the former is reasonably set to 6 ps,[13] while the latter is given by the value, which varies with P, measured by PL experiments we performed on the operating device. Simulated results, shown in Fig. 2, obtained for our prototypical resonant-phonon terahertz emitting device at a phonon in-plane wavenumber $q = 4.2\times10^{+4}\,cm^{-1}$, show a very good agreement with measured data, indicating how the out-of-equilibrium LO phonon population affects the electro-optical device performances.[13] Conversely, our theoretical approach also allows us to directly investigate the features of the LO phonon distribution over the wavevector q, due to the non-trivial coupling with the "hot" electron subsystem.

Figure 3 shows the comparison between the LO and IF-TO like phonon occupation numbers in the investigated THz QC laser (sample a) as a function of P. Four regions, clearly correlated with features in the transport measurements (Fig. 3(b)) can be identified. At $P < 2.5$ W, (region I) band structure calculations show that the energy of the injector doublet remains more than 6 meV lower than that of the upper state and transport proceeds via injection into level 3. Under these conditions, the phonon population is approximately thermal. As carriers start being injected into the upper state (region II) ($2.5 < P < 3.3$ W), a non-equilibrium phonon population arises in our structure that increases as the injector level 1 approaches the resonance with subband 5 ($P = 3.4$ W). The large negative discontinuity in the differential resistance at the onset of region III ($2.5 < P < 3.3$ W) indicates that the laser threshold is reached, while the population inversion becomes clamped at the onset for stimulated emission.[14] Correspondingly, the slope of N vs power decreases implying that the photon emission extracts part of the input power, efficiently cooling both the electron[15] and optical phonon subsystems. This behavior is very similar to that observed for hot electrons in a terahertz QCL.[15] A further proof of the optical origin of the latter effect is the fact that this change disappears when the same measurements are performed on a non-lasing device (sample b) as shown in Fig. 2. Finally, in region IV (P > 4.3 W) lasing ceases, as revealed by the sudden jump in the differential resistance (Fig. 3(b)). In this roll-off regime, the voltage drop in each stage and the associated subband structure become ambiguous.

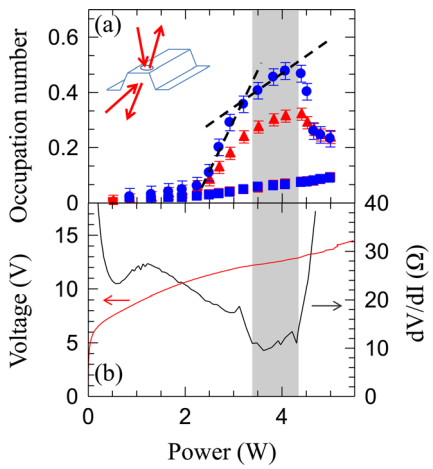

FIG. 3. (Color online) (a) LO (●) and IF-TO (▲) phonon occupation numbers in a terahertz quantum cascade laser plotted as a function of P, together with the corresponding equilibrium phonon populations (■). (b) Voltage-power and differential resistance vs power characteristics collected at $T_H = 57$ K, while driving the QCL in continuous wave mode. The inset shows a schematic diagram of the employed experimental configuration. The arrows show the direction of the incident and scattered photons in the Raman processes. The grey area show the lasing regime.

[1]P. Lugli and S. M. Goodnick, Phys. Rev. Lett. **59**, 716 (1987).
[2]B. S. Williams, H. Callebaut, S. Kumar, Q. Hu, and J. L. Reno, Appl. Phys. Lett. **82**, 1015 (2003).
[3]G. Scamarcio, M. S. Vitiello, V. Spagnolo, S. Kumar, B. S. Williams, and Q. Hu, Physica E **40**, 1780 (2008).
[4]W. E. Bron, *Non-equilibrium Phonons in Non-metallic Crystals*, edited by W. Eisenmenger and A. A. Kaplyanskii (North-Holland, Amsterdam, 1986).
[5]S. Kumar, B. S. Williams, S. Kohen, Q. Hu, and J. L. Reno, Appl. Phys. Lett. **84**, 2494 (2004).
[6]M. S. Vitiello, G. Scamarcio, V. Spagnolo, B. S. Williams, S. Kumar, Q. Hu, and J. L. Reno, Appl. Phys. Lett. **86**, 111115 (2005).
[7]M. S. Vitiello, G. Scamarcio, V. Spagnolo, C. Worral, H. E. Beere, D. A. Ritchie, C. Sirtori, J. Alton, and S. Barbieri, Appl. Phys. Lett. **89**, 131114 (2006).
[8]M. S. Vitiello, G. Scamarcio, and V. Spagnolo, IEEE J. Sel. Top. Quantum Electron. **14**, 431 (2008).
[9]M. S. Vitiello, G. Scamarcio, V. Spagnolo, J. Alton, S. Barbieri, C. Worral, H. E. Beere, D. A. Ritchie, and C. Sirtori, Appl. Phys. Lett. **89**, 021111 (2006).
[10]R. C. Iotti, F. Rossi, M. S. Vitiello, G. Scamarcio, L. Mahler, and A. Tredicucci, Appl. Phys. Lett. **97**, 033110 (2010).
[11]T. Schmielau and M. F. Pereira, Jr., Appl. Phys. Lett. **95**, 231111 (2009).
[12]T. Kubis, C. Yeh, P. Vogl, A. Benz, G. Fashing, and C. Deutsch, Phys. Rev. B **79**, 195323 (2009).
[13]J. Shah, *Ultrafast Spectroscopy of Semiconductors and Semiconductor Nanostructures* (Springer, Berlin, 1998).
[14]C. Sirtori, F. Capasso, J. Faist, A. L. Hutchinson, D. L. Sivco, and A. Y. Cho, IEEE J. Quantum Electron. **34**, 1722 (1998).
[15]M. S. Vitiello, G. Scamarcio, J. Faist, G. Scalari, C. Walther, H. Beere, and D. A. Ritchie, Appl. Phys. Lett. **94**, 021115 (2009).